Using LiDAR data to identify geometrically feasible roofs for UAM alternate landing

Simon Carlswärd[1)†], Yantong Dou[2)], Alon Efrat[3)], Kien Huynh[1)], Valentin Polishchuk[1)], Leonid Sedov[1)], and Yu Zhang[2)]

[1)] *Flight Logistics unit, Communications and Transport Systems, Linköping University, Sweden*
[2)] *Department of Civil and Environmental Engineering, University of South Florida, USA*
[3)] *Computer Science, The University of Arizona, USA*
[†] *email: simca98@liu.se*

We process urban LiDAR scan data, aiming to identify locations on buildings' roofs whose geometry allows the rooftops to host an alternate landing site for an Urban Air Mobility vehicle during a contingency/emergency situation. The feasibility of a site is governed by two parameters (the size of the vehicle and the rooftop height difference within a potential site), and we show how the parameter values influence availability of the sites: we report on computational experiments with real-world data from two neighborhoods in Stockholm (city center with many cluttered and sloped roofs, and outskirts of the city with many flat roofs) in Sweden, and from a US city with varying roof geometry. We also present a graphical user interface that allows one to see interactively how the parameters change the roof areas available for the landing. Use of alternate landing sites supports EASA's requirements for VTOL aircraft route planning, and may be part of emergency management plans for U-space service providers and of contingency procedures for the operators. Our work thus contributes to development of decision support tools which may help the stakeholders in making urban air mobility networks a reality.

Key Words : Vertiports, Alternate landing sites, Geometric algorithms, Urban LiDAR data

1. Introduction

Passenger-carrying aerial vehicles are envisioned to become part of Urban Air Mobility (UAM) aka Advanced Air Mobility (AAM) or Innovative Air Mobility (IAM) in Europe [1, 2]. UAM promises to improve accessibility and increase the speed of urban travel by offering a more efficient alternative to congested ground transport.

Safety is of utmost importance in urban air travel, inherited from the highest standards in conventional aviation. However, despite the extensive technical and organizational measures aimed at ensuring low failure rates during the flight, contingencies and emergencies still occur, which may require aircraft to perform an unexpected landing at an available location. In conventional aviation, ICAO's Extended Diversion Time Operations (EDTO) requirements [3] (formerly known as ETOPS: Extended-range Twin-engine Operations Performance Standards) stipulate that at any point during the flight, the aircraft has an alternate airport (Fig. 1) reachable within certain time (called Maximum Diversion Time).

For UAM, analogous requirements are formulated, e.g., in the European Union Aviation Safety Agency's (EASA's) Special Condition for small-category Vertical Take-Off and Landing (VTOL) aircraft [4]: it puts the controlled emergency landing (CEL) requirement on the Basic category vehicles and continued safe flight and landing (CSFL) on aircraft in the Enhanced category. EASA suggests that every U-plan (the UAM analogue of flightplan in conventional aviation [5]) specifies potential alternate landing sites (ALSs) for the whole duration of the flight (Fig. 2).

ALSs may also be a part of the emergency management plans which U-space service providers (USSPs) shall have according to EU U-space regulation 664 [7, Article 6.8]. On the operators' side, such sites may enter the contingency procedures which operators should provide to USSPs [7, Article 15.2].

Note that even though we mostly refer to EU documents above, ALSs are relevant for UAM on other continents just as well. Indeed, sustainable urban mobility plan (SUMP) of many cities around the world feature a long-term vision of developed UAM operations, seamlessly weaved into transportation network, and flight safety is high on the agenda of the stakeholders everywhere.

1.1. Comparison with related work

Placing vertiports for *nominal* UAM operations is an active research subject; space constraints do not allow us to survey all the papers in detail, so we mention only some literature. Monteleone, Dhamodharasamy Sundarraj, Pedretti, Rylko, Berlingieri, Quaranta and Setti [8] presented an inter-

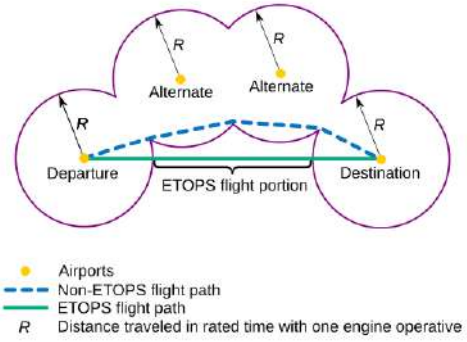

Fig. 1. Reproduced from "ETOPS rating flight path" by Vladsinger, Wikimedia Commons, licensed under CC BY-SA 4.0; resized.

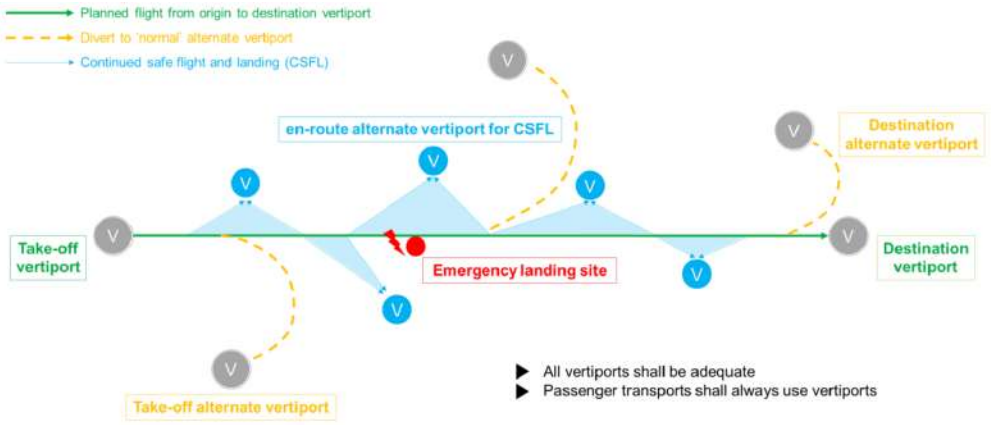

Figure F-1. En-route alternate vertiport for CSFL

Fig. 2. Reproduced from EASA [6, Figure F-1].

disciplinary framework to vertiport design. Lippoldt, Preis and Bogenberger [9] proposed a data-driven approach to vertiport placement, leveraging mobility survey data to identify high-demand locations for UAM infrastructure. Kotwicz Herniczek and German [10] suggested a scalable combinatorial methodology for vertiport placement optimization, focusing on maximizing demand for UAM commuting services; their method integrates commuter flow data, congestion modeling, and economic factors to determine optimal vertiport locations. Yoon, Jeong, Lee, Kim and Yoon [11] studied locations for highway-transfer vertiports. Lu, Zeng, Wei, Wu and Jiang [12] developed a system for evaluation and optimization of vertiport siting. Wu and Zhang [13] examined the network design of UAM on-demand service, presenting an algorithm to determine the optimal locations of vertiports, user allocation to vertiports, and vertiport access- and egress-mode choices while considering the interactions between vertiport locations and potential UAM travel demand. Earlier studies on vertiport placement include [14, 15, 16, 17, 18, 19, 20, 21, 22, 23].

While vertiport siting for nominal conditions is a booming research area, localization of ALSs has received less attention (our work intends to contribute to filling the gap):

- Gonzales [24] used LiDAR data to find large rectangles with the same height values on roofs. We also use LiDAR scans, but we do not demand a feasible ALS location to be completely flat (i.e., to have the same height): on the contrary, the height difference Δ that we allow within an ALS is one of our main parameters and is a user-tunable input in our GUI (Δ accounts for noise in the data and also for possibility of landing on an inclined and not perfectly even surface); in addition, instead of grouping feasible ALS locations into polygons (as done in [24]), We evaluate candidate ALS centers on a regular 1×1 m grid over each usable roof surface. Nearby LiDAR points are used to estimate local roof height variation at each grid center (this is not a strict improvement over [24]: even though our analysis is more fine-grained, polygons may present a better overall picture for a quick overview of ALSs, and also require less storage).
- Castango and Atkins [25] converted LiDAR scan into RGB raster files which were fed, along with satellite images, into Convolutional Neural Network and Random Forest algorithms to classify roofs into seven shapes, of which flat roofs were labeled suitable for landing. In this paper we use exact algorithms, not Machine Learning (ML) or Neural Network (NN) techniques.
- More generally, there is an abundance of ML/NN tools (not related to UAM) to partition Digital Elevation Maps (DEMs) into approximately same-height rectangles: Region-Growing and Random Sample Consensus (RANSAC) [26, 27], clustering, k-means and fussy k-means [28], Cross-line Element Growth [29], etc.; in UTM, Ref. [30] partitioned DEMs into approximately same-height rectangles as means of addressing the AGL/AMSL dilemma (how to measure height in metropolitan areas: above ground or the mean sea level). We emphasize, however, that partitioning a roof (representing the roof as the union of *pairwise-disjoint* parts) is less suitable for ALS localization than covering the roof (i.e., representing the roof as the union of *possibly overlapping* parts) – we are looking for ALS for a single vehicle, not a full vertihub of ALSs for multiple vehicles each with a separate landing site.
- Tang, Xu, Inalhan and Tsourdos [31] routed drones close to ALSs. However, the experiments in [31, Section V.A] were performed on synthetic data: in particular, ALSs were just points in a square, without connection to any rooftops (or to any buildings or any city). Results like ours (i.e., obtained from real data) may enhance a continuation of work like [31] by providing realistic input to routing algorithms.

While a well developed UAM system is envisioned to feature high levels of automation and digitalization (cf. the

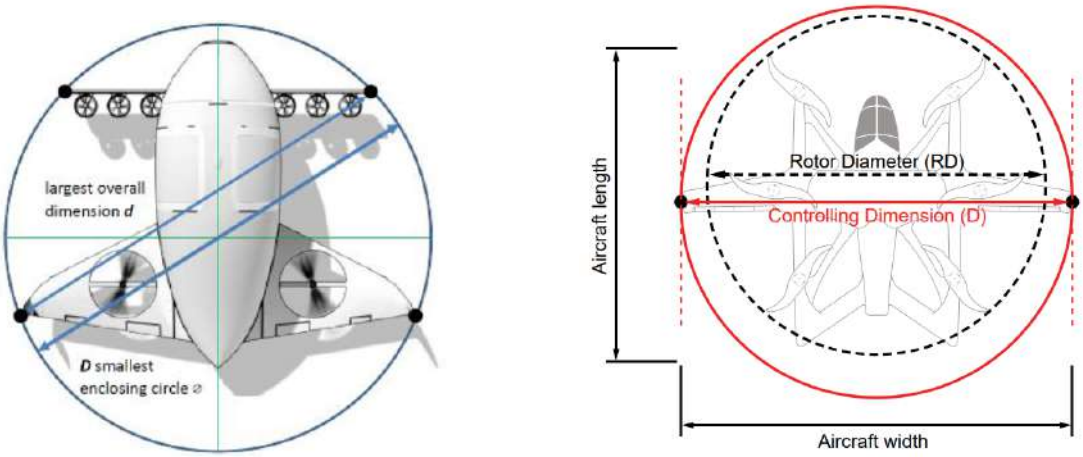

Fig. 3. Left: reproduced from EASA [32, Figure 1]. Right: reproduced from FAA [33, Figure 1-1].

definition of "U-space airspace" in EU's Regulation 664, as a geographical zone where operations must rely on "digital services and automation of functions" [7, Article 2]), frequent interaction with stakeholders is likely inevitable, at least in the initial stages of UAM implementation. We are not aware of much effort devoted to interfaces facilitating consultation with the authorities on UAM landing sites questions, which would help bridging the gap between researchers and decision makers (two exceptions are an interactive tool for identifying ground locations compliant with EASA's vertiport envelopes [6] which was recently reported in [34], and [25] which used humans for labeling training samples). In this paper we also report on a graphical user interface (GUI) which allows the user to see the buildings and play with the ALS parameters, understanding their influence on the available sites (unlike [34], we do not check whether the landing trajectory would be clear from obstacles, we only make sure there is space to land: this is because we are locating sites for contingency/emergency events when standard landing envelopes might not be followed, and instead other types of descents like ballistic, glide, parachute, and flyaway [35, 36, 37, 38] may become more relevant – studying them is outside the scope of this paper).

1.2. Roadmap

The next section describes the data which we used as the input. Section 3 explains the processing pipeline. We present the results of evaluating available ALS locations in Section 4 Section 5 links to the GUI for the reader to play with it. We conclude with some alleys for future research in Section 6

2. Data

We read in data from [39] – an open geospatial dataset available under a Creative Commons Zero (CC0) license. The dataset consists of a 3D point cloud collected using airborne laser scanning (LiDAR) over Sweden since 2018. The data has a typical density of 1–2 points per square meter and each point is classified (e.g., ground, water, bridges, or noise). It is distributed in LAZ format (an open-source, lossless compressed version of the LAS file format [40]) in 2.5×2.5 km tiles and uses the SWEREF 99 TM coordinate system. For the US, we used tiles from USGS National Map [41] which has density of more than 25 points per square meter. The high quality of the US data let us focus on a small area (one block), as large regions would require too much computation time to process.

Next, we took building footprints from Open Street Maps (OSM) [42]; the footprints are a set of polygons. Using OSM info, we removed buildings tagged as 'school', 'hospital', 'police', 'childcare', 'kindergarten', but kept e.g., 'residential buildings' (if needed, these choices are easy to modify in our code). We analyzed each polygon separately, restricting the LiDAR data to it, as described in the next section. Note that OSM contributors occasionally mark roofs as "flat", but this crowd-sourced data is far from complete and thus can not be used as a reliable source for determining ALSs (Fig. 4); in any case, it does not help with identifying feasible and infeasible locations on each *single* roof (OSM only lets one indicate that the whole roof is flat), which is our focus.

Our code includes a simple data quality checker. E.g., for every building, we take its OSM footprint polygon and check LiDAR data close to the boundary of the polygon: we verify that on different sides of the boundary (i.e., inside vs outside the polygon) LiDAR data has points of substantially different heights (the roof of the building vs the ground). We work only with data that passed our checks. While LiDAR data are noisy, our workflow applies lightweight filtering and geometric preprocessing before evaluating landing feasibility, including point filtering, roof-surface estimation, interpolation, and grid-based sampling. A full treatment of LiDAR denoising and uncertainty analysis is outside the scope of this paper.

3. Processing

There are two geometric factors that determine feasibility of a location for alternate landing: the area should be large enough to accept the vehicle, and the area should be flat

Fig. 4. Left: Orange are roofs marked as flat in OSM (© OpenStreetMap contributors, ODbL). Middle: It is seen on a Bing Maps bird's eye screenshot that the roofs are not all flat (resized; Microsoft product screenshot reprinted with permission from Microsoft Corporation; map data: © 2026 TomTom, © OpenStreetMap contributors). Right: Our GUI (described in Section 5) confirms that not all marked roofs are available: the wireframe on the LiDAR data shows the buildings and the green are feasible ALS centers.

enough (the height difference of points within the area should be small) to prevent the landed aircraft from tipping over. These requirements aim at formally capturing the intuition that only a "large flat" area should be designated as an ALS.

Typically, the 2D footprint of a UAM drone is modeled with a disk. Figure 3 illustrates the similar ways in which EASA [32] and FAA [33] determine the drones characteristic dimension, called the *D-value*, from the vehicles physical measurements. According to "Ground Risk and Landing Site Management Deliverable 3.2" [43] from the EU's Horizon 2020 project "Enabling sustainable AiR MObility in URban contexts via emergency and medical services (AiRMOUR)": "As for the largest overall dimensions on the ground for the site, they are equal to the D-value of the drones that shall land on it." Following estimations of UAM vehicles size from available sources [44, Table 3], we set the default diameter of the ALS disk to be D=6.5m (there is noting special about this choice; the diameter is a tunable parameter in our experiments and GUI). For the maximum allowable height difference within the disk, our default value is Δ =1m. This is completely arbitrary, but, again, both in our experiments and in the GUI, we run through multiple different values for D and Δ: from D_{min}=0 to D_{max}=20m for D, and from Δ_{min}=0 to Δ_{max}=3m for Δ. Naturally, we do not claim that any combination (D, Δ) make sense in practice, but we rather err on the side of investigating too much of the parameter space than too little. In particular, one use of setting D to a practically unreasonable value of 0 is that in this case, the area available for ALS centers essentially shows the total area of the roofs. Note also that looking for a perfectly flat ALS ($\Delta = 0$) is not only impractical (UAM vehicles will likely be able to tolerate some $\Delta > 0$), but is also doomed because LiDAR data is noisy: setting $\Delta > 0$ accounts for errors in the LiDAR measurements (quantifying precision of LiDAR data obtained from various sources and at various times is a rich research area in itself, far outside our scope).

Every roof polygon P (obtained from OSM – see previous section) is processed as follows. The *features* of P are its vertices and its (open) edges (i.e., edges without their endpoints, the vertices). We build the Voronoi diagram VD of the features, i.e., the decomposition of P into cells such that for all points inside one cell σ, the closest feature f is the same (Fig. 5). In particular, being the closest means that f will be the first feature hit by a growing disc centered at any point within σ.

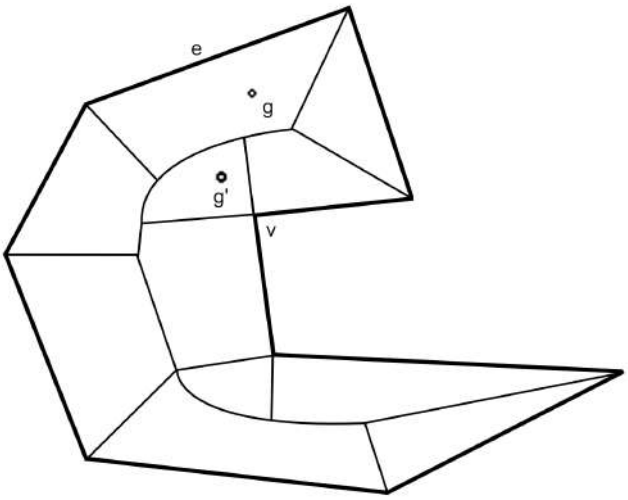

Fig. 5. Voronoi diagram of the features of the polygon: all points in the cell of g have the edge e as the closest feature; all points in the cell of g' have the vertex v as the closest feature (illustration by the authors).

We lay out a square grid within P, with granularity of 1m, and for every grid point g, assign the height interpolated from the nearby LiDAR data points. We also determine in which cell of VD the point g lies – this indicates the feature f of P, closest to g. Knowing f, we compute the distance d_g from g to f.

The main procedure of our algorithm is growing the disc $D_g(r)$ centered at g, starting from the radius r=$D_{min}/2$. We continue growing the disc until r reaches $D_{max}/2$ or the distance d_g from g to the boundary of P, whichever is smaller. That is, either the diameter of the disk reaches the preset maximum D-value of interest or the disk of larger diameter

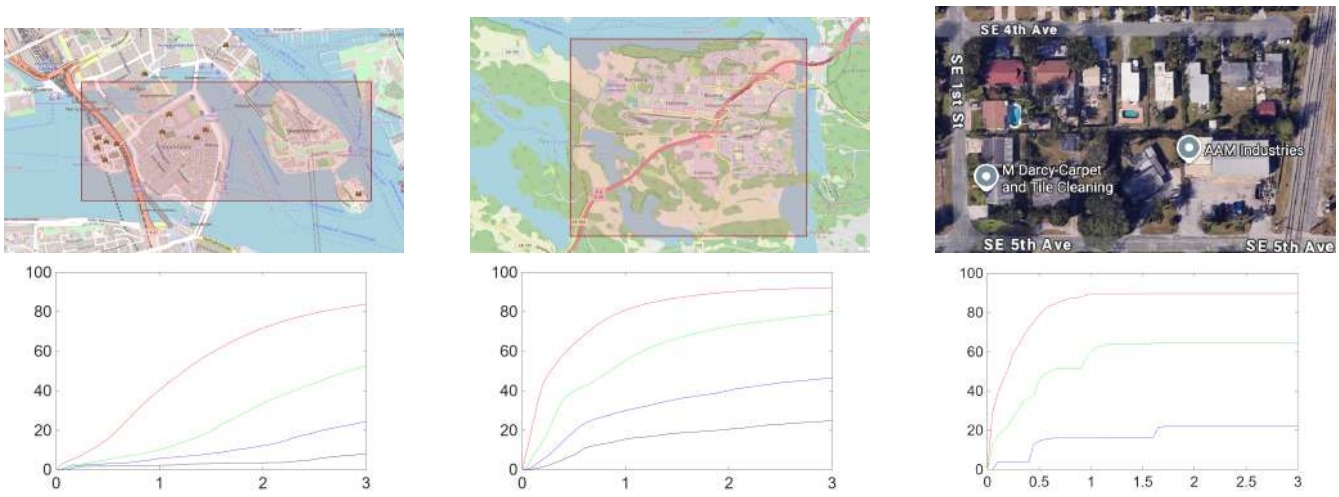

Fig. 6. Left: Stockholm city center [45]. Middle: Stockholm suburb [46]. Left and middle locator maps use OpenStreetMap data (© OpenStreetMap contributors, ODbL). Right: Google Maps screenshot of a block in Boynton Beach, Florida (resized; imagery and map data: © Google and its data providers). Top: The processed areas are the red shaded rectangles. Bottom: Percentage of geometrically feasible ALS roof area as function of Δ, for various D: red, green, blue and black curves are for D = 4, 8, 12 and 18m resp. (the black curve is not seen on the bottom right because it is 0 for any Δ – the roofs are small).

becomes infeasible as an ALS because it would go outside the roof. During the growth, we maintain the minimum, $h(r)$, and maximum, $H(r)$, height of the LiDAR points within $D_g(r)$: when the disc hits a new point p, with height $\ell(p)$, we either keep $h(r)$ and $H(r)$ unchanged (if $h(r) \le \ell(p) \le H(r)$) or update $h(r)$ or $H(r)$ with $\ell(p)$ (if $\ell(p) < h(r)$ or $\ell(p) > H(r)$ resp.). In particular, this way we record the height difference $\Delta_g(r) = H(r) - h(r)$ of points within $D_g(r)$ as function of r (we stop growing the disc when $\Delta_g(r)$ reaches $\Delta_{\max}$). The function stores the full information on the pairs (D, Δ), for which g is a center of feasible ALS – and this is all we need both for measuring the dependence of available ALS areas on D and Δ (reported in the next section), and for our GUI (detailed in Section 5).

4. Results

Figure 6 shows the available ALS areas as functions of D and Δ for various use cases, described in Table 1. In Stockholm city center the ALS-friendly area grows slowly with Δ (Fig. 6, left) because there are many older houses with sloped Scandinavian roofs, and Δ needs to increase quite substantially before a disk is marked as a feasible ALS. In Stockholm outskirts district of Norra Botkyrka the available area grows faster with Δ (Fig. 6, middle): the neighborhood features standardized buildings with mostly flat roofs from a large public housing program implemented in Sweden ca. 1970. The roofs in Boynton Beach were small, so for large D of 18m there is no ALS space at all; for smaller D, the area grows in "steps", also due to the small roof size.

5. The GUI

We coded a graphical user interface (GUI) for visualizing the results from the previous section on a small scale. The users can play with the GUI online at `https://hyrax.se/vertidisc/`. The interface has a small Leaflet map with Esri World Imagery, focused on the buildings presented on the main canvas. The map includes the usual scrolling, zooming and panning fea- tures that allow the user to inspect the chosen geographical area. The user may adjust the canvas view by rotating/zooming, turning the grid and the axes on/off, see any building as a triangulated surface or a frame, view the original LiDAR data point cloud, etc.

The main elements of the GUI are the sliders for D and Δ. Moving them shows which points on the roofs may host the center of the ALS disk, and also the disks themselves (both the centers and the discs views can be toggled on and off). Figure 7 shows snapshots of the GUI for different values of the parameters. It can be seen how larger D implies less areas available for ALS centers (even though every feasible ALS is larger).

The code for the GUI (as well as for generating the results, like in Section 4) is openly available at [47]. We recommend using the GUI on a touchscreen (Fig. 8), allowing several people to play with it together.

6. Conclusion and Future work

We processed LiDAR data to identify geometrically feasible locations for ALSs on roofs; we also presented a GUI for the users to play with the ALS parameters. Our work contributes to development of decision support tools which may help the authorities and operators to reason about possible UAM network implementation by getting a picture of roofs in the city, which have geometry allowing one to potentially host an ALS for UAM.

We emphasize our focus on geometric feasibility which is a key aspect in ALS localization: if a UAM vehicle does not fit into a certain space on a roof, it will not be able to land there. Our results may thus be viewed more as an *exclusion*: the locations that we *do not* label as feasible are *not* suitable places for ALS. At the same time we understand that some places which we identify as geometrically feasible ALSs,

Neighborhood	Number of buildings	Total roof area, sq. m	Average roof area, sq. m	Locator map link
Gamla Stan	ca. 500	208060	416	[45]
Norra Botkyrka	ca. 2500	1101183	440	[46]
Boynton Beach	ca. 20	ca. 2924	88	-

Table 1. : Use cases

Fig. 7. Available ALS centers locations (dark green) and disks (blue). From left to right: D = 6.5m, Δ = 1m; D = 6.5m, Δ = 0.5m; D = 15m, Δ = 1m.

Fig. 8. The GUI on a touchscreen.

Fig. 9. A 3D printed tile from model of Norrköping city in Sweden

in reality might not host an ALS for a variety of reasons. In the future work we will present our tool to city planners and local experts, so they exclude even more places as potential ALSs; we will also try to get a better understanding which data-driven approaches may help with refining ALS localization – knowing roof surface composition (whether its sturdy enough to withstand landing of different types of aircraft), building classification (we already exclude kindergartens, prisons, and similar places), etc: at the very least, tools like ours may help the authorities understand which roofs may need to be checked/approved/retrofitted for ALS at all. For better usability, we will also make a user interface for our calculations for the users to upload their footprint and LiDAR datasets, choose level of downsampling (if any), have a view of the locations, and making our tools more user friendly in general (instead of running our code is from a terminal command window, as we do for this paper). Another direction for future research is to project out GUI on a 3D printed model of the city (Fig. 9), so people would be able to see ALSs in 3D.

While we focused on the 3D geometry of roofs, we ignored the 3D consideration of the landing trajectory: a vehicle in distress may deviate from standard landing procedures. Similarly, we did not take into account environmental and social aspects (like noise), which are less of a concern in an emergency/contingency situation. Our overall postulate, motivating this work is that it is better to land on a roof (even if it is not easily accessible, does not have power supply to quickly recharge the vehicle, etc.) than to fall onto the ground, posing a hazard to uninvolved people. Future work may extend our techniques with checking whether the landing path is clear of obstacles (as was done with ground vertiport siting

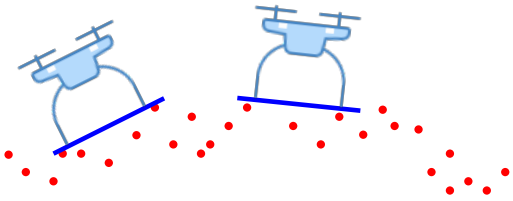

Fig. 10. A 2D view: red are LiDAR points sampled from the roof and blue is the bottom of the aircraft (drone icon is from icons8.com). The slope of the aircraft depends on where it lands and is determined by the slope of the hyperplane through the touch points.

in [34]) and consider routing the UAM vehicles so that at any point of the route they have an ALS in the vicinity (e.g., feeding our ALSs into algorithms of [31]). The UAM flights may be quite long, implying that we would have to process data on a larger scale, to obtain the feasible ALS areas for buildings along a planned UAM route.

Note that while vertiports for nominal UAM operations may be scattered quite scarcely throughout a city (depending on travel demand, electricity supply, access infrastructure, etc.) and may be decided on a case-by-case basis with a lot of human oversight, the potential ALSs may need to be more dense, hedging, in particular, against global events (communication outage, sudden inclement weather, emergency medical services, urban airspace reservation for government operations, etc.) that may require many UAM aircraft to simultaneously land somewhere. This motivates the development and use of tools, like the ones presented in this paper, for automated computerized identification of potential ALSs.

On the technical side, one may question our definition of a feasible ALS as the one with a small height difference (Δ): for instance, a roof that is perfectly flat except for 1 point at $-\infty$ is a bona fide landing site, but is infeasible by our definition (because $\Delta = \infty$ for such a roof). Recall that we wanted small Δ to ensure that the UAM aircraft does not fall after the landing. What indeed matters for that is the slope of the aircraft that stands on an ALS. In particular, if the bottom of the aircraft is modeled as a disk (which may be a good first model, before considering the exact geometry of the vehicle's chassis or skids), the slope of the aircraft is defined by the slope of the hyperplane through the roof points on which the aircraft stands (Fig. 10). If one had perfectly precise LiDAR data, one could in principle scroll through all triples of LiDAR points and check whether the triple could support the landing: is there a disk supported by the triple, does the disk's center (of mass) lie inside the triangle determined by the triple, do all the points in the triple lie close to the disk boundary (to support the balance) – and take into account the physics otherwise (friction, etc.). Defining and computing the supporting hyperplanes and the slopes from noisy LiDAR data, as well as considering the physics of the landing, is left for future research; this paper is about geometric considerations.

Acknowledgments

This work is partially supported by the Swedish Transport Administration and by the Florida Department of Transportation (FDOT) through Project No. BED25-729-1. The contents of this paper reflect the views of the authors, who are responsible for the facts and accuracy of the information presented herein. The contents do not necessarily reflect the official views or policies of the Florida Department of Transportation.

References

1) EASA, "Innovative Air Mobility for City Transport Ecosystems," 2025, accessed: 2025-03-30. [Online]. Available: https://www.easa.europa.eu/en/domains/drones-air-mobility/drones-air-mobility-landscape/IAM-for-City-Transport-Ecosystems

2) ——, "Innovative Air Mobility Hub," 2025, accessed: 2025-03-30. [Online]. Available: https://www.easa.europa.eu/en/domains/drones-air-mobility/drones-air-mobility-landscape/innovative-air-mobility-hub

3) ICAO, *Extended Diversion Time Operations (EDTO) Manual*, 2017, document Number 10085. [Online]. Available: https://www.icao.int/MID/Documents/2020/EDTO%20Workshop/10085_cons_en.pdf

4) EASA, "Special Condition for small-category VTOL aircraft ," 2022.

5) SESAR, "Concept of Operations for European U-space Services - Extension for Urban Air Mobility (CORUS-XUAM)," 2023.

6) EASA, "Prototype Technical Specifications for the Design of VFR Vertiports for Operation with Manned VTOL-Capable Aircraft Certified in the Enhanced Category," 2022.

7) EC, "Commission implementing regulation (eu) 2021/664 of 22 april 2021 on a regulatory framework for the u-space," 2021.

8) F. Monteleone, N. Dhamodharasamy Sundarraj, O. Pedretti, A. Rylko, F. Berlingieri, G. Quaranta, and G. Setti, "An interdisciplinary research perspective for tackling vertiport design and developmental challenges," in *Delft International Conference on Urban Air Mobility (DICUAM)*, 2024, pp. 1–12.

9) K. Lippoldt, L. Preis, and K. Bogenberger, "Vertiport placement method based on mobility survey data," in *32nd Congress of the International Council of the Aeronautical Sciences (ICAS)*, 2021.

10) M. T. Kotwicz Herniczek and B. J. German, "Scalable Combinatorial Vertiport Placement Method for an Urban Air Mobility Commuting Service," *Transportation Research Record*, vol. 2678, no. 10, pp. 1624–1641, 2024.

11) D. Yoon, M. Jeong, J. Lee, S. Kim, and Y. Yoon, "Integrating Urban Air Mobility with Highway Infrastructure: A Strategic Approach for Vertiport Location Selection in the Seoul Metropolitan Area," *arXiv preprint arXiv:2502.00399*, 2025.

12) Y. Lu, W. Zeng, W. Wei, W. Wu, and H. Jiang, "Vertiport location selection and optimization for urban air mobility in complex urban scenes," *Aerospace*, vol. 12, no. 8, p. 709, 2025.

13) Z. Wu and Y. Zhang, "Integrated network design and demand forecast for on-demand urban air mobility," *Engineering*, vol. 7, no. 4, pp. 473–487, 2021.

14) K. R. Antcliff, M. D. Moore, and K. H. Goodrich, "Silicon valley as an early adopter for on-demand civil vtol operations," in *16th AIAA Aviation Technology, Integration, and Operations Conference*, 2016, p. 3466.

15) P. D. Vascik and R. J. Hansman, "Evaluation of key operational constraints affecting on-demand mobility for aviation in the los angeles basin: ground infrastructure, air traffic control and noise," in *17th AIAA Aviation Technology, Integration, and Operations Conference*, 2017, p. 3084.

16) C. Courtin, M. J. Burton, A. Yu, P. Butler, P. D. Vascik, and R. J. Hansman, "Feasibility study of short takeoff and landing urban air mobility vehicles using geometric programming," in *2018 Aviation Technology, Integration, and Operations Conference*, 2018, p. 4151.

17) J. N. Robinson, M.-D. R. Sokollek, C. Y. Justin, and D. N. Mavris, "Development of a methodology for parametric analysis of stol airpark geo-density," in *2018 Aviation Technology, Integration, and Operations Conference*, 2018, p. 3054.

18) M. Daskilewicz, B. German, M. Warren, L. A. Garrow, S.-S. Boddupalli, and T. H. Douthat, "Progress in vertiport placement and estimating aircraft range requirements for evtol daily commuting," in *2018 Aviation Technology, Integration, and Operations Conference*, 2018, p. 2884.

19) D. J. Peisen, W. T. Sampson, L. J. Labelle, B. M. Sawyer, J. Ludders, S. V. Berardo, R. J. Dyment, S. W. Ferguson, R. M. Winick, and C. R. Bragdon, "Analysis of vertiport studies funded by the airport improvement program (aip)," MIT, Tech. Rep., 1994.

20) H. Tang, Y. Zhang, V. Mohmoodian, and H. Charkhgard, "Automated flight planning of high-density urban air mobility," *Transportation Research Part C: Emerging Technologies*, vol. 131, p. 103324, 2021.

21) M. M. Nodehi, M. Almasabi, S. Mahmoudinazlou, J. Post, Y. Dou, and Y. Zhang, "A research approach for integrating advanced air mobility into transportation planning," *Available at SSRN 4960705*, 2024.

22) Y. An, B. Zeng, Y. Zhang, and L. Zhao, "Reliable p-median facility location problem: two-stage robust models and algorithms," *Transportation Research Part B: Methodological*, vol. 64, pp. 54–72, 2014.

23) Y. An, Y. Zhang, and B. Zeng, "The reliable hub-and-spoke design problem: Models and algorithms," *Transportation Research Part B: Methodological*, vol. 77, pp. 103–122, 2015.

24) C. J. D. Gonzalez, "Rooftop-place suitability analysis for urban air mobility hubs: A gis and neural network approach," Master's thesis, Universidade NOVA de Lisboa (Portugal), 2020.

25) J. Castagno and E. Atkins, "Roof shape classification from lidar and satellite image data fusion using supervised learning," *Sensors*, vol. 18, no. 11, p. 3960, 2018.

26) R. Albano, "Investigation on roof segmentation for 3d building reconstruction from aerial lidar point clouds," *Applied Sciences*, vol. 9, no. 21, p. 4674, 2019.

27) D. Chen, L. Zhang, J. Li, and R. Liu, "Urban building roof segmentation from airborne lidar point clouds," *International journal of remote sensing*, vol. 33, no. 20, pp. 6497–6515, 2012.

28) J. Shan and A. Sampath, "Building extraction from lidar point clouds based on clustering techniques," in *Topographic Laser Ranging and Scanning*. CRC Press, 2017, pp. 421–444.

29) T. Wu, X. Hu, and L. Ye, "Fast and accurate plane segmentation of airborne lidar point cloud using cross-line elements," *Remote Sensing*, vol. 8, no. 5, p. 383, 2016.

30) L. Sedov, V. Polishchuk, and V. Acuna, "Altitude zoning for utm," *10th SESAR Innovation Days*, vol. 2020, 2020.

31) Y. Tang, Y. Xu, G. Inalhan, and A. Tsourdos, "An integrated approach for dynamic capacity management service in u-space," in *14th USA/Europe ATM R&D Seminar*, 2021.

32) EASA, "Vertiports. Prototype Technical Specifications for the Design of VFR Vertiports for Operation with Manned VTOL-Capable Aircraft Certified in the Enhanced Category," 2022.

33) FAA, "EB 105A, Vertiport Design, Supplemental Guidance to AC 150/5390-2D, Heliport Design," 2024, accessed: 2025-03-30. [Online]. Available: https://www.faa.gov/airports/engineering/engineering_briefs/eb_105a_vertiports

34) B. Josefsson, K. Huynh, A. Lemetti, V. Polishchuk, and L. Sedov, "Geometric vertiport localization: Uam procedural envelopes in a cityscape," in *Digital Avionics Systems Conference*, 2025.

35) A. la Cour-Harbo, "Ground impact probability distribution for small unmanned aircraft in ballistic descent," in *2020 International Conference on Unmanned Aircraft Systems (ICUAS)*. IEEE, 2020, pp. 1442–1451.

36) Y. Su, Y. Xu, and G. Inalhan, "A comprehensive flight plan risk assessment and optimization method considering air and ground risk of UAM," in *2022 IEEE/AIAA 41st Digital Avionics Systems Conference (DASC)*. IEEE, 2022, pp. 1–10.

37) Q. Jiao, Y. Liu, Z. Zheng, L. Sun, Y. Bai, Z. Zhang, L. Sun, G. Ren, G. Zhou, X. Chen, and Y. Yan, "Ground Risk Assessment for Unmanned Aircraft Systems Based on Dynamic Model." *Drones*, vol. 6, no. 11, p. 324, 2022.

38) J. Kim, "Enhancing Safety, Efficiency, and Resilience in Advanced Air Mobility Through Geofencing, Contingency Landing Management, and Optimized Network Strategies," Ph.D. dissertation, University of Michigan, 2024.

39) Lantmäteriet, "Laserdata nedladdning, skog," https://geotorget.lantmateriet.se/geodataprodukter/laserdata-nedladdning-skog, 2026, accessed: 2026-04-01.

40) Wikipedia contributors, "LAS file format — Wikipedia, the free encyclopedia," https://en.wikipedia.org/wiki/LAS_file_format, 2026, [Online; accessed 1-April-2026].

41) U.S. Geological Survey, "The national map," https://apps.nationalmap.gov/downloader/, 2026.

42) OpenStreetMap contributors, "Planet dump retrieved from https://planet.osm.org ," https://www.openstreetmap.org, 2017.

43) K. Wigler, "Ground risk and landing site management deliverable 3.2," 2022, AiRMOUR project.

44) J. Lee, U. Huh, P. Wei, and K. Song, "Efficient urban air mobility vertiport operational plans considering on-ground traffic environment," *Sustainability*, vol. 17, no. 11, p. 5054, 2025.

45) S. Carlswärd, "Gamla stan locator map," http://tiny.cc/vertma/gamlastan_locator_map.html, 2026.

46) ——, "Norra botkyrka locator map," http://tiny.cc/vertma/nbotkyrka_locator_map.html, 2026.

47) ——, "Alternate landing sites," https://github.com/carlsward/Vertiports, 2026.